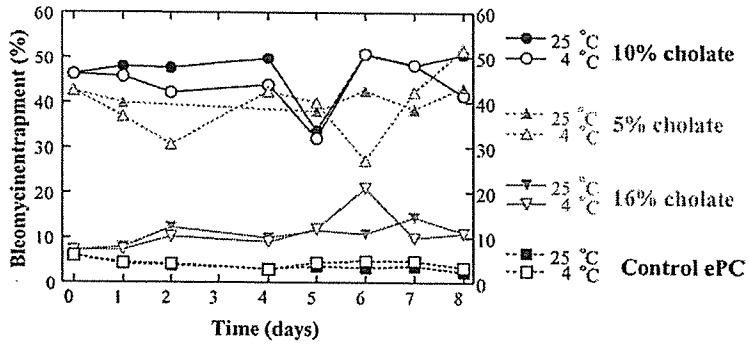

Fig. 3. Comparing bleomycin entrapment (%) in 'low dose' Bleosome™ formulations incorporating various concentrations of sodium cholate against control liposomes without any sodium cholate, whilst being stored in PBS, at refrigerated (4 °C) and room temperatures (25 °C) over 8 days ($n=1$).

sizes (low dose 163.5 ± 20.1 nm, $n=3$; empty vesicles 189.9 ± 7.3 nm, $n=3$; high dose 139.4 ± 5.7 nm, $n=3$) (data not shown) were seen to have returned to the expected range of 150–200 nm. Subsequent stability tests were carried out at room temperature (25 °C) on three separate preparations of Bleosome™ incorporating 10% (w/w) sodium cholate and data from each preparation have been individually plotted to clearly demonstrate their relatively unchanged characteristics after 7 days. It was observed that initial entrapment levels afforded by the same formulation fluctuated between 12 and 32% (Fig. 4). However, only the 32% preparation (first preparation) was used for purification and cell toxicity testing, procedures, which were carried out on the same day as Bleosome™ production. Hence, it was possible to accurately compare the precise data on initial entrapment concentration and efficiency and average particle size (Fig. 4) of the original Bleosome™ preparation against their respective values after purification (as above and in Section 3.2), prior to cell toxicity testing.

3.2. Purification by gel chromatography

Fig. 5 shows a bimodal distribution (□) with the peak on the left-hand representing the elution of bleomycin entrapped in Bleosome™ and the right-hand peak signifying elution of free bleomycin in the solution. Also shown is the corresponding average particle diameter (nm) for each 1 ml fraction (right axis) from fractions 10–25 (●) of the eluent. A significant reduction in average particle size was observed

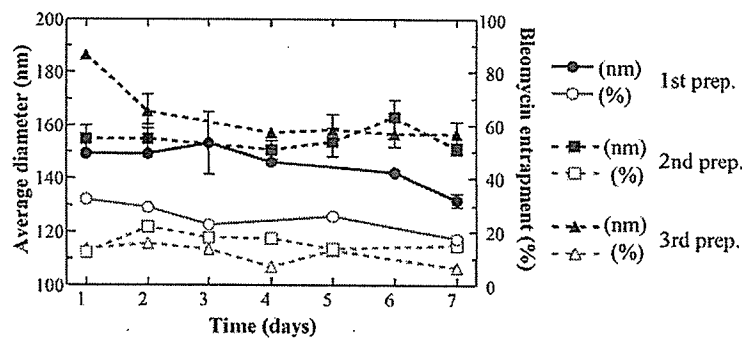

Fig. 4. Average diameter (nm) (mean ± S.D., $n=3$) and bleomycin entrapment levels (%) ($n=1$) of three separate preparations of 'high dose' Bleosome™ featuring 10% (w/w) sodium cholate, in 1/10 PBS during storage over 7 days at room temperature (25 °C). Each trace represents the bleomycin retention or particle size profile of 'high dose' Bleosome™ in one preparation.

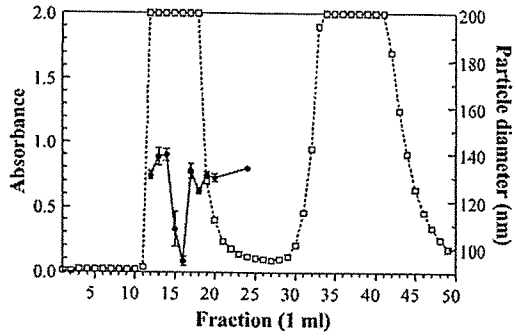

Fig. 5. Gel-filtration chromatography separation (□) of bleomycin entrapped in 'low dose' Bleosome™ incorporating 10% (w/w) sodium cholate and unentrapped, free bleomycin. Fractions 14–16 were pooled to form a stock supply of 'high dose' Bleosome™ for testing on keratinocytes ($n=1$). Average particle diameter (nm) for fractions 10–25 (●) have been plotted to show size variation within the liposomal component of the eluent (mean ± S.D., $n=3$).

for fraction 15 (108.1 ± 7.4 nm, $n=3$) and fraction 16 (94.6 ± 2.0 nm, $n=3$). Theoretically, the largest particles ought to elute first and smaller particles would be retarded the most, eluting thereafter. It can be seen that fraction 16 possessed the smallest average size compared to the general range of 130–140 nm. When fractions 14, 15 and 16 were pooled together to form a stock suspension of 'high dose' Bleosome™, the resulting average size returned to the median of approximately 140 nm (Section 3.1). However, if it was necessary to supply only the smallest liposomes, then fraction 16 could be isolated and specifically used for this purpose.

3.3. Toxicity studies on human keratinocyte lines

Two different concentrations of liposomal bleomycin were prepared for keratinocyte toxicity studies: Bleosome™ preparations containing a low concentration (low dose) of bleomycin (22.3 ± 8.2 μg/ml; $n=3$) and a high concentration (high dose) of bleomycin (1091.5 ± 25.8 μg/ml; $n=3$). The average particle size of these high-dose preparations did not differ significantly from the low-dose Bleosome™ and both versions lay within the desired range of 150–200 nm (Section 3.1).

'Low dose' Bleosome™ were tested on NEB-1 and SCC cells, but it was found that the levels of bleomycin inside these liposomes were of a concentration that was too low to exert a clearly lethal action on both cell types (data not shown). Subsequently, it was necessary to manufacture a new batch of Bleosome™, and by substantially increasing the initial amount of bleomycin used for entrapment, liposomal bleomycin levels were elevated 50-fold in order to obtain a 'high dose' for eliciting lethal effects in keratinocytes.

Fig. 6 compares the toxicity of bleomycin in Bleosome™ against free bleomycin solution on NEB-1 and SCC cells. It was clear that the liposomal form of bleomycin does have a progressively lethal effect on both types of keratinocytes as the concentration of liposomal bleomycin was increased. In order to quantatively compare the degree of toxicity, it was convenient to compare the dose required to kill half the population of cells present (LD_{50}). From Fig. 6, the estimated LD_{50}

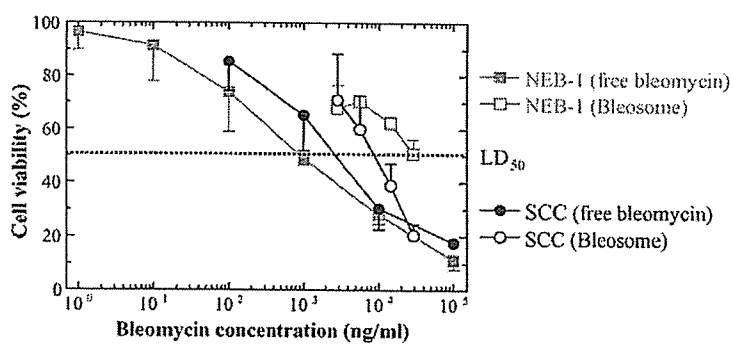

Fig. 6. LD_{50} toxicity study of 'high dose' Bleosome™ incorporating 10% (w/w) sodium cholate (empty symbols) and free bleomycin in culture medium (solid symbols) on NEB-1 human keratinocytes, immortalised with HPV-16 (Storey et al., 1988) (NEB-1, square symbols) and keratinocytes derived from human squamous cell carcinoma (SCC, circle symbols) (mean ± S.D., $n=3$).

values for immortalised keratinocytes (NEB-1) were found to be 30 μg/ml for Bleosome™ and 1 μg/ml for free bleomycin solution. From Fig. 6, the estimated LD_{50} values for SCC cells were found to be 9 μg/ml for Bleosome™ and 3 μg/ml for free bleomycin solution.

4. Discussion

Bleosome™ preparations generally seemed to be less potent than free bleomycin solution against both NEB-1 and SCC cell lines, except for the 30 μg/ml dose of liposomal bleomycin on SCC cells. Encapsulating bleomycin molecules inside vesicles naturally partitioned them away from as well as hindered their presentation to keratinocytes. This compartmentalisation of the cytotoxin most likely limits the amount of drug available to the keratinocytes in vitro. Although minor, some leakage was seen to occur from Bleosome™ samples during storage at room temperature (Fig. 4). It has yet to be determined whether cell death was caused by bleomycin that had leaked out, or from extensive drug release when the liposomes themselves had been destabilised, whilst adsorbing onto cell surfaces or during ingestion by keratinocytes. The 30-fold difference in LD_{50} between Bleosome™ and free bleomycin solution on NEB-1 cells (Fig. 6) suggests that even a small amount of drug leakage from a 30 μg/ml preparation of Bleosome™ might release sufficient bleomycin to potentially cause a substantial reduction in the population of NEB-1 cells. However, this factor seems to be diminished when SCC cultures were treated with Bleosome™ since the LD_{50} value was only three times higher than that of unencapsulated drug (Fig. 6). This indicates that SCC cells were more susceptible to bleomycin and Bleosome™ treatment than NEB-1 cells. Since both cell lines were treated from the same batch of Bleosome™, it may be assumed that their difference in sensitivity to drug treatment might be due to other factors, as discussed below.

The origins of SCC and NEB-1 cells are dissimilar. The SCC tumour was excised and dissociated samples of malignant keratinocytes were then cultivated and the cells that subsequently emerged exhibited immortality, possibly as a result of genetic changes such as a chromosomal loss. In contrast, NEB-1 cells were immortalised in vitro by the co-operative transforming properties of E6 and E7 genes of the HPV-16 genome (Barbosa and Schlegel, 1989; Hawley-Nelson et al., 1989): E6 disrupts p53 tumour suppressor protein expression (Scheffner et al., 1990; Werness et al., 1990) and E7 disrupts the PKB pathway (Dyson et al., 1989). These pathways had become inactivated in both instances, but the mechanisms behind their ability for uncontrolled proliferation may be inhibited by bleomycin to varying degrees. It has yet to be determined whether the activity of Bleosome™ on keratinocytes led to cell death by way of apoptosis or necrosis. Nonetheless, the E6 protein of a number of different cutaneous HPV-types has been found to block the epidermal apoptotic response to UV radiation (Jackson and Storey, 2000) and HPV-positive NMSC displayed greatly reduced apoptotic rates when compared to HPV-negative NMSC (Jackson et al., 2002). However, despite the high expression of p53 in many tumours, patients with cutaneous SCC had low prevalence of anti-p53 antibodies (Moch et al., 2001). This may be related to the prevalence of wild-type p53 over mutant p53, where the tumour is HPV-positive. These findings suggest that part of the signalling pathway responsible for initiating apoptosis may be absent or substantially impaired in one or both of the cell lines.

Bleomycin hydrolase is a member of the papain superfamily of cysteine proteases (Takeda et al., 1996b). It is responsible for the intracellular inactivation of bleomycin (Umezawa et al., 1974). Bleomycin hydrolase activity can be measured by quantifying metabolites of active bleomycin B2, and significantly it has been demonstrated that bleomycin hydrolase is expressed in normal skin, but not in squamous cell carcinoma (Lazo et al., 1982; Takeda et al., 1999). Moreover, it has been directly demonstrated that overexpression of human bleomycin hydrolase protected Chinese hamster ovary cells against bleomycin-induced chromosomal damage in G2 phase of the cell cycle (Lefterov et al., 1998). Whether these differences in Bleosome™ toxicity between the NEB-1 and SCC cells was due to a difference in expression and/or activity of bleomycin hydrolase remains to be determined. Bleomycin hydrolase activity can be inhibited by iodoacetic acid, *N*-ethylmaleinimide (NEM) and *p*-chloromercuribenzoic acid (pCMB) as well as divalent cations such as Cu^{2+}, Cd^{2+}, Hg^{2+} and Zn^{2+} (Takeda et al., 1996a). As yet, relatively little is known about metabolic factors that might influence

chromosomal DNA damage caused by bleomycin and further investigations will be required to ascertain the determining intracellular operations that elevate NEB-1 cell resistance to liposomal bleomycin to three times that of SCC cells (Fig. 6).

Purification of Bleosome™ by gel-filtration chromatography resulted in a product suitable for research purposes, but the yield was low and the liposomal concentration of bleomycin was diluted at least five-fold. It became necessary to employ much higher quantities of lipids and drug at the outset of production in order to obtain a viable product after elution from the gel column. The expense of the raw materials may rule out this method of purification when scaling up batch production for clinical trials. Ultra-centrifugation is an obvious choice, but further testing would be required in order to fine-tune this method to achieve a better yield of stable highly loaded liposomes.

The fact that storage of Bleosome™ at 4 °C did not change their stability over storage at room temperature (Figs. 2 and 3) has an important practical aspect in any subsequent commercial manufacturing and storage of Bleosome™ preparations: Bleosome™ can be kept at room temperature for at least a week without significant detriment. Mild storage conditions may suffice and no further optimisation of the formulation with respect to stability is required. These circumstances may need to be reconsidered if the Bleosome™ suspension will be diluted into a solid or semi-solid preparation, such as a gel/cream. Compatibility assessment of gel/cream excipients on liposome stability would then be required.

5. Conclusions

Ultra-deformable liposomes containing bleomycin (Bleosome™) were stable at room temperature and did not exhibit significant changes to their drug load or average particle size for at least 7 days. Bleosome™ exerted a lethal effect on human keratinocytes cell lines and a cell line derived from a primary carcinoma in vitro when loaded with sufficient bleomycin. The cell line derived from squamous cell carcinoma seemed to be more susceptible to Bleosome™ than HPV-immortalised keratinocytes (NEB-1). Potency of Bleosome™ loaded with 30 μg/ml bleomycin on SCC cells was similar to that of free bleomycin solution, but significantly fewer NEB-1 cells than SCC cells were killed at this concentration. This distinction suggests that Bleosome™ containing high levels of bleomycin may possess a passive specificity for the in vitro demise of SCC over NEB-1 cells.

Acknowledgements

Kent G. Lau was funded by an International Research Fellowship from the Nagai Foundation (Tokyo, Japan) and Alan Storey was funded by Cancer Research, UK. We wish to thank Ms. Kem Ojeh (London, UK) for her advice on culturing keratinocytes.

References

Aszalos, A., Crawford, P., Vollmer, P., Kantor, N., Alexander, T., 1981. High-performance liquid chromatographic determination of components of bleomycin preparations. J. Pharm. Sci. 70, 878–880.

Barbosa, M.S., Schlegel, R., 1989. The E6 and E7 genes of HPV-18 are sufficient for inducing two-stage in vitro transformation of human keratinocytes. Oncogene 4, 1529–1532.

Cevc, G., Blume, G., 2003. Biological activity and characteristics of triamcinolone-acetonide formulated with the self-regulating drug carriers, transfersomes. Biochim. Biophys. Acta 1614, 156–164.

Cevc, G., Gebauer, D., Stieber, J., Schatzlein, A., Blume, G., 1998. Ultraflexible vesicles, transfersomes, have an extremely low pore penetration resistance and transport therapeutic amounts of insulin across the intact mammalian skin. Biochim. Biophys. Acta 1368, 201–215.

Cevc, G., Schatzlein, A., Richardsen, H., 2002. Ultradeformable lipid vesicles can penetrate the skin and other semi-permeable barriers unfragmented. Evidence from double label CLSM experiments and direct size measurements. Biochim. Biophys. Acta 1564, 21–30.

Dyson, N., Howley, P.M., Munger, K., Harlow, E., 1989. The human papilloma virus-16 E7 oncoprotein is able to bind to the retinoblastoma gene product. Science 243, 934–937.

El Maghraby, G.M., Williams, A.C., Barry, B.W., 2001a. Skin delivery of 5-fluorouracil from ultradeformable and standard liposomes in-vitro. J. Pharm. Pharmacol. 53, 1069–1077.

El Maghraby, G.M., Williams, A.C., Barry, B.W., 2001b. Skin hydration and possible shunt route penetration in controlled estradiol delivery from ultradeformable and standard liposomes. J. Pharm. Pharmacol. 53, 1311–1322.

Fiedler, H.-P., Wachter, J., 1991. High-performance liquid chromatographic determination of bleomycins. J. Chromatogr. 536, 343–347.

Hawley-Nelson, P., Vousden, K.H., Hubbert, N.L., Lowy, D.R., Schiller, J.T., 1989. HPV16 E6 and E7 proteins cooperate to immortalize human foreskin keratinocytes. EMBO J. 8, 3905–3910.

Hofer, C., Gobel, R., Deering, P., Lehmer, A., Breul, J., 1999. Formulation of interleukin-2 and interferon-alpha containing ultradeformable carriers for potential transdermal application. Anticancer Res. 19, 1505–1507.

Jackson, S., Storey, A., 2000. E6 proteins from diverse cutaneous HPV types inhibit apoptosis in response to UV damage. Oncogene 19, 592–598.

Jackson, S., Ghali, L., Harwood, C., Storey, A., 2002. Reduced apoptotic levels in squamous but not basal cell carcinomas correlates with cutaneous human papillomavirus expression. Br. J. Cancer 87, 319–323.

Kim, A., Lee, E.H., Choi, S.H., Kim, C.K., 2004. in vitro and in vivo transfection efficiency of a novel ultradeformable cationic liposome. Biomaterials 25, 305–313.

Lau, K.G., Chopra, S., Maitani, Y., 2003. Entrapment of bleomycin in ultra-deformable liposomes. S. T. P. Pharm. Sci. 13, 237–239.

Lazo, J.S., Boland, C.J., Schwartz, P.E., 1982. Bleomycin hydrolase activity and cytotoxicity in human tumors. Cancer Res. 42, 4026–4031.

Lefterov, I.M., Koldamova, R.P., King, J., Lazo, J.S., 1998. The C-terminus of human bleomycin hydrolase is required for protection against bleomycin-induced chromosomal damage. Mutat. Res. 421, 1–7.

Moch, C., Moysan, A., Lubin, R., de la Salmoniere, P., Soufir, N., Galisson, F., Vilmer, C., Venutolo, E., Le Pelletier, F., Janin, A., Basset-Seguin, N., 2001. Divergence between the high rate of p53 mutations in skin carcinomas and the low prevalence of anti-p53 antibodies. Br. J. Cancer 85, 1883–1886.

Morley, S.M., D'Alessandro, M., Sexton, C., Rugg, E.L., Navsaria, H., Shemanko, C.S., Huber, M., Hohl, D., Heagerty, A.I., Leigh, I.M., Lane, E.B., 2003. Generation and characterization of epidermolysis bullosa simplex cell lines: scratch assays show faster migration with disruptive keratin mutations. Br. J. Dermatol. 149, 46–58.

Purdie, K.J., Sexton, C.J., Proby, C.M., Glover, M.T., Williams, A.T., Stables, J.N., Leigh, I.M., 1993. Malignant transformation of cutaneous lesions in renal allograft patients: a role for human papillomavirus? Cancer Res. 53, 5328–5333.

Scheffner, M., Werness, B.A., Huibregtse, J.M., Levine, A.J., Howley, P.M., 1990. The E6 oncoprotein encoded by human papillomavirus types 16 and 18 promotes the degradation of p53. Cell 63, 1129–1136.

Storey, A., Pim, D., Murray, A., Osborn, K., Banks, L., Crawford, L., 1988. Comparison of the in vitro transforming activities of human papillomavirus types. EMBO J. 7, 1815–1820.

Takeda, A., Higuchi, D., Yamamoto, T., Nakamura, Y., Masuda, Y., Hirabayashi, T., Nakaya, K., 1996a. Purification and characterization of bleomycin hydrolase, which represents a new family of cysteine proteases, from rat skin. J. Biochem. (Tokyo) 119, 29–36.

Takeda, A., Masuda, Y., Yamamoto, T., Hirabayashi, T., Nakamura, Y., Nakaya, K., 1996b. Cloning and analysis of cDNA encoding rat bleomycin hydrolase, a DNA-binding cysteine protease. J. Biochem. (Tokyo) 120, 353–359.

Takeda, A., Nonaka, M., Ishikawa, A., Higuchi, D., 1999. Immunohistochemical localization of the neutral cysteine protease bleomycin hydrolase in human skin. Arch. Dermatol. Res. 291, 238–240.

Umezawa, H., Hori, S., Sawa, T., Yoshioka, T., Takeuchi, T., 1974. A bleomycin-inactivating enzyme in mouse liver. J. Antibiot. 27, 419–424.

Werness, B.A., Levine, A.J., Howley, P.M., 1990. Association of human papillomavirus types 16 and 18 E6 proteins with p53. Science 248, 76–79.

Cancer Gene Therapy (2005) 12, 796–809

www.nature.com/cgt

Folate-linked nanoparticle-mediated suicide gene therapy in human prostate cancer and nasopharyngeal cancer with herpes simplex virus thymidine kinase

Yoshiyuki Hattori,[1] and Yoshie Maitani[1]

[1]*Institute of Medicinal Chemistry, Hoshi University, Ebara 2-4-41, Shinagawa-ku, Tokyo 142-8501, Japan.*

For targeted gene delivery to human prostate cancer LNCaP and PC-3 cells and nasopharyngeal cancer KB cells, we developed a folate-linked nanoparticle (NP-F), and evaluated the potential of NP-F-mediated suicide gene therapy in the cells and xenografts with herpes simplex virus thymidine kinase (HSV-tk) and connexin 43 (Cx43). An NP-F-plasmid DNA complex (NP-F nanoplex) showed high DNA transfection efficiency in KB, LNCaP and PC-3 cells. Cell growth inhibition in the presence of ganciclovir (GCV) was enhanced with HSV-tk and Cx43 genes in LNCaP cells. In suicide gene therapy, the tumor growths of KB and LNCaP xenografts were significantly inhibited when an NP-F nanoplex of the HSV-tk gene, and HSV-tk and Cx43 genes, respectively, was injected intratumorally and GCV was administered intraperitoneally. These findings suggested that the NP-F is a potential target vector in prostate and nasopharyngeal cancer for suicide gene therapy.
Cancer Gene Therapy (2005) **12,** 796–809. doi:10.1038/sj.cgt.7700844; published online 13 May 2005

Keywords: prostate cancer; nasopharygeal cancer; cationic nanoparticles; folic acid; in vivo; suicide gene

Prostate cancer is a significant problem and is reported to be the leading cancer diagnosed in males.[1] Androgen sensitivity and prostate-specific antigen (PSA) production are hallmarks of the prostatic phenotype, both benign and malignant, which are of clinical importance. Thus, androgen-sensitive, PSA-producing cancer models are desirable for study; however, most cell lines are considered inadequate models because they lack the characteristics of androgen sensitivity and PSA production. At present, only the PSA-positive prostate cancer cell line, LNCaP, is available.[2] Currently, androgen deprivation therapy is the most effective treatment for advanced prostate cancer. However, the deprivation therapy eventually fails, because the metastatic prostate cancer within an individual patient is composed heterogeneously of clones of both androgen-dependent and -independent cancer cells. Therefore, androgen-independent cancer cell lines, for example, PC-3, are utilized as an androgen-independent cancer model.

As an alternative treatment, suicide gene therapy in prostate cancer has been reported, in which a gene can be introduced locally using an adenoviral vector into cancer cells, making them sensitive to a drug that is normally nontoxic.[3–5] The suicide genes used often encode enzymes that metabolize nontoxic prodrugs into toxic metabolites. One of the most frequently used suicide genes is the herpes simplex virus thymidine kinase (HSV-tk) gene,[6] which phosphorylates a prodrug, ganciclovir (GCV), into a toxic form. A powerful characteristic of HSV-tk/GCV therapy is that the transduction of a small fraction of the tumor cells with the suicide gene can result in widespread tumor cell death (bystander effect). The cell to cell transfer of HSV-tk-activated GCV between HSV-tk-transduced tumor cells and neighboring unmodified cells via gap junctions is a major mechanism of the bystander effect.[7] Gap junctions are composed of connexin subunits and connect the cytoplasmic domains of contacting cells, allowing ionic and metabolic exchange between them. However, many cancer cell lines are deficient in gap junctions.[8] Such a deficiency, which is also found in human prostate tumors,[9] can limit the extent of the bystander effect in suicide gene therapy. However, the bystander effect has been reported to be enhanced by introducing a connexin gene with the HSV-tk gene *in vitro*.[7]

The development of nonviral and tumor-selective delivery vectors for *in vivo* gene transfer is necessary for the clinical application of therapeutic genes. Synthetic vectors such as lipid nanoparticles (liposome and emulsion) have become an attractive choice due to their lack of immunogenicity, the potential for tissue-specific targeting, relative safety and a relatively easy large-scale production. For targeted delivery to tumors, the folate receptor (FR) has been used since FR has been identified as a marker for ovarian carcinomas[10] and has also been found to be frequently overexpressed in a wide range of other types of tumors.[11] Folic acid retains its receptor-binding and endocytotic properties when covalently linked to a wide

Received July 14, 2004.
Address correspondence and reprint requests to: Professor Y Maitani, Institute of Medicinal Chemistry, Hoshi University, Ebara 2-4-41, Shinagawa-ku, Tokyo 142-8501, Japan.
E-mail: yoshie@hoshi.ac.jp

variety of molecules. Liposomes conjugated to a folate ligand via a polyethyleneglycol (PEG)-spacer have been used for the delivery of chemotherapeutic agents and plasmid DNA to receptor-bearing tumor cells, for example, human oral cancer KB cells.[12–15] However, the use of a folate ligand as a targeting ligand to deliver DNA has not been successful in *in vivo* gene therapy.[13,14] Folate-linked liposomes administered intraperitoneally showed just the transfection activity of a reporter gene (luciferase gene) in a disseminated intraperitoneal tumor model.[13] An FR-targeted lipoplex caused no increase in accumulation when systemically administered.[14]

In human prostate tissue, high-affinity folate binding protein has also been characterized.[16] However, the type of folate binding protein expressed in human prostate has not been reported. Therefore, the use of a folate ligand as a targeting ligand to deliver DNA is a potential strategy for the treatment of prostate cancer.

Previously, we reported that a folate-linked cationic nanoparticle could deliver DNA with high transfection efficiency into KB cells via FR and into LNCaP cells where the expression of FRs was not observed,[17] but did not provide enough transfection efficiency in an *in vivo* experiment. In this study, we developed new folate-linked nanoparticle (NP-F) to enhance the gene expression in LNCaP, PC-3 and KB cells, and evaluated the transfection with NP-F from the cytotoxic effects in the cells and xenografts with HSV-tk and connexin 43 (Cx43) genes. The therapeutic effect of the HSV-tk genes was observed in both KB and LNCaP tumor xenografts.

Materials and methods

Plasmid constructions

pCMV-tk was constructed using a cDNA fragment (589 bp) coding for a cytomegalovirus (CMV) promoter amplified by PCR with a pEGFP-C1 plasmid (Clontech, CA) containing a green fluorescent protein (GFP) reporter gene under the control of the CMV promoter as a template, and the following CMV promoter-specific primers: CMV promoter forward primer (5′ ATGG TACCTAGTTATTAATAGTAATCAA) and CMV promoter reverse primer (5′ TCAAGCTTGATCTGACGG TTCACTAAAC). The forward and reverse primers, respectively, contained *Kpn*I and *Hind*III restriction sites. The cDNA coding for bp 1–1131 of HSV-tk was amplified by PCR using the pLXSN plasmid containing the HSV-tk gene with a midkine promoter[18] as a template with the following HSV-tk-specific primers: HSV-tk forward primer (5′ ATCAATGGaccATGGCTTCGTA CCCC) and HSV-tk reverse primer (5′ CATCTAGATCA GTTAGCCTCCCCCAT). The forward primer contained a 3 bp optimal Kozak sequence (in lowercase letters) together with an *Nco*I restriction site (underlined). The reverse primer coded for bp 1114–1131 of HSV-tk with an *Xba*I restriction site (underlined). After the HSV-tk cDNA amplification, this cDNA was digested with *Nco*I and *Xba*I and ligated into an *Nco*I/*Xba*I-digested pGL3-enhancer (Promega, Madison, WI). The plasmid was then digested with *Kpn*I and *Hind*III, and ligated with the CMV promoter cDNA.

In the construction of pSV40-Cx43, total RNA was isolated from KB cells using NusleoSpin RNA II (Macherey-Nagel, Germany). First-strand cDNA was synthesized from 5 μg of total RNA after denaturation for 5 minutes at 65°C using 50 pmol of random primer, 0.5 mM dNTP and 5 U of AMV reverse transcriptase XL (Takara Shuzo Co., LTD, Japan). The reaction was performed at 41°C for 1 hour in a 20 μl volume. The cDNA coding bp 1–1149 of human Cx43 was amplified by PCR using the synthesized cDNA from KB cells as a template and the following Cx43-specific primers: Cx43 forward primer (5′ ATCAATGGaccATGGGTGACTG GAGCGCCT) and Cx43 reverse primer (5′ CATCTAGA CTAGATCTCCAGGTCATCAG.). The forward primer contained a 3-bp optimal Kozak sequence (in lowercase letters) together with an *Nco*I restriction site (underlined). The reverse primer coded for bp 1129–1149 of Cx43 with an *Xba*I restriction site (underlined). After the Cx43 cDNA amplification, this cDNA was digested with *Nco*I and *Xba*I and was ligated into an *Nco*I/*Xba*I-digested pGL3-control (Promega, Madison, WI) with the simian virus (SV40) promoter.

A protein-free preparation of the plasmid was purified following alkaline lysis using maxiprep columns (Qiagen, Hilden, Germany).

Preparation of FITC-labeled oligonucleotide DNA

The FITC-labeled 30-mer randomized oligonucleotide and its compliment (FITC-ODN) were synthesized with a phosphodiester backbone (Sigma Genosys Japan, Hokkaido, Japan). The two oligonucleotides were mixed and annealed to make double-stranded DNA.

Preparation, size and ζ-potential of nanoparticles and nanoplexes

Folate-polyethyleneglycol-distearoylphoshatidylethanolamine (f-PEG-DSPE) (mean molecular weight of PEG: 2 kDa) was synthesized.[17] 3([*N*-(*N*′,*N*′–dimethylaminoethane)-carbamoyl] cholesterol (DC-Chol) was purchased from Sigma Chemical Co. (St Louis, MO). Tween 80 (99% purity) was obtained from NOF Co. Ltd (Tokyo, Japan). Nanoparticles were prepared by a modified ethanol injection method as previously described.[17] For example, in the case of NP-2F (NP-F), DC-Chol:Tween 80:f-PEG-DSPE at 93:5:2 molar ratio (10:1.3:1.3, weight) was dissolved in about 5 ml of ethanol, and then the ethanol was removed with a rotary evaporator till 1–2 ml was left. Next, a constant volume of water was added to the ethanol solution. The nanoparticles formed instantly after further evaporation of the residual ethanol. The concentration of DC-Chol was adjusted to 1 mg/ml in the final nanoparticle suspension with water. Then, the nanoparticle suspension was filtered through 0.45-μm Millex-HA filters (Millipore, Cork, Ireland) to sterilize it. In 1,1′-dioctadecyl-3,3,3′,3′-tetramethylindocarbocyanine perchlorate (DiI) (Lambda Probes & Diagnostics, Graz,

Austria)-labeled nanoparticles, DiI was incorporated at 0.04 mol% of total lipid.

Based on a preliminary experiment, the optimized ratio of cationic lipid to DNA was determined as 3:1. The nanoplex at a charge ratio (+/−) of 3/1 and Tfx20 (Promega, Madison, WI) lipoplex at a charge ratio (+/−) of 2/1 of cationic lipid to DNA were formed by addition of each nanoparticle (9.5 μl) or Tfx20 (6 μl) to 2 μg of DNA with gentle shaking and leaving at room temperature for 10 minutes. The particle size distributions and the ζ-potentials were measured by the dynamic light scattering method and the electrophoresis light scattering method, respectively (ELS-800, Otsuka Electronics Co., Ltd, Osaka, Japan), at 25°C after the dispersion was diluted to an appropriate volume with water. The stability of nanoparticles and nanoplexes was assessed by measuring changes in size after 30 days and dilutions in 10 or 50% serum, respectively.

In vitro *experiments*

Cell culture. LNCaP cells were supplied by the Department of Urology, Keio University Hospital (Tokyo, Japan). PC-3 and KB cells were from the Cell Resource Center for Biomedical Research, Tohoku University (Miyagi, Japan). A human cervix carcinoma cell line, HeLa 229, was supplied by the Department of Virology, Toyama Medical and Pharmaceutical University (Toyama, Japan). A human hepatoblastoma cell line, HepG2, was obtained from the Riken Cell Bank (Ibaraki, Japan). All the cell lines used in this study were grown in a folate-deficient RPMI 1640 medium (Life Technologies Inc., Grand Island, NY) supplemented with 10% heat-inactivated fetal bovine serum (Life Technologies Inc.) and kanamycin (100 μg/ml) at 37°C in a 5% CO_2 humidified atmosphere.

Luciferase gene transfection in the cells and luciferase assay

The pCMV-luc encoding the luciferase gene was supplied by Dr Tanaka at the Mt Sinai School of Medicine (NY, USA). Cell cultures were prepared by plating cells in a 35-mm culture dish 24 hours prior to each experiment. The nanoplex at a charge ratio (+/−) of 3/1 and Tfx20 lipoplex at a charge ratio (+/−) of 2/1 of cationic lipid to DNA were formed by addition of each nanoparticle (9.5 μl) or Tfx20 (6 μl) to 2 μg of DNA with gentle shaking and leaving at room temperature for 10 minutes. Each nanoplex was diluted in 1 ml of complete medium and then incubated for 24 hours. Luciferase expression was measured according to the luciferase assay system (Pica gene luciferase assay kit, Toyo Ink Mfg Co. Ltd, Tokyo, Japan) as previously reported.[17]

RT-PCR analysis of FR expression in the cells. Total RNA was isolated from LNCaP, PC-3, KB, HeLa and HepG2 cells, using NusleoSpin RNA II as described in the section above. Total RNA from tumor human prostate tissue was obtained from Ambion Inc. (Austin, TX). RNA yield and purity were checked by spectrometric measurement at 260 and 280 nm and RNA electrophoresis, respectively. For RT-PCR, a 25-μl reaction volume contained 1 μl of synthesized cDNA, 10 pmol of each specific primer pair and 0.25 U of Ex *Taq* DNA polymerase (Takara Shuzo Co., LTD) with a PCR buffer containing 1.5 mM $MgCl_2$ and 0.2 mM of each dNTP. The profile of PCR amplification consisted of denaturation at 94°C for 0.5 minutes, primer annealing at 58°C for 0.5 minutes and elongation at 72°C for 1 minute for 25 cycles. PCRs of the housekeeping gene β-actin, FRs (FR-α, -β, -γ) and reduced folate carrier (RFC) were performed at the same cycle run for all samples. The PCR products for FRs, RFC and β-actin were analyzed by 1.5% agarose gel electrophoresis in a Tris-Borate-EDTA (TBE) buffer. The products were visualized by ethidium bromide staining.

Flow cytometric analysis. KB and LNCaP cell cultures were prepared by plating cells in a 35-mm culture dish 24 hours prior to each experiment. In competition assay, 9.5 μl of DiI-labeled NP-F was mixed with 2 μg of FITC-ODN and then diluted in 1 ml of folate-deficient RPMI medium containing 10% serum. KB cells were incubated with the nanoplex in the presence or absence of 1 mM folic acid for 3 hours. In cellular association based on FITC-ODN, 9.5 μl of NP-F was mixed with 2 μg of FITC-ODN and then diluted in 1 ml of the medium. LNCaP and PC-3 cells, respectively, were incubated with the nanoplex for 3 or 24 hours. After incubation, the dishes were washed two times with 1 ml of PBS (pH 7.4) to remove any unbound nanoplex, and the cells were detached with 0.25% trypsin. The cells were centrifuged at 1500 *g*, and the supernatant was discarded and resuspended with PBS containing 0.1% bovine serum albumin (BSA) and 1 mM EDTA. The suspended cells were directly introduced into a FACSCalibur flow cytometer (Becton Dickinson, San Jose, CA) equipped with a 488-nm argon ion laser. Data for 10,000 fluorescent events were obtained by recording forward scatter (FSC), side scatter (SSC) and green (530/30 nm) and red (585/42 nm) fluorescences.

Confocal microscopy. LNCaP and PC-3 cells were plated into 35-mm culture dishes. DiI-labeled NP-F (9.5 μl) was mixed with 2 μg of FITC-ODN and pEGFP plasmid coding enhanced GFP under the control of the CMV promoter (Clontech, CA), and then diluted in 1 ml of medium supplemented with 10% serum. The cells were incubated with the mixture for 24 hours. Examinations were performed with a Radiance 2100 confocal laser scanning microscope (BioRad, CA), as previously described.[17] For DiI, maximal excitation was performed with the 543-nm line of an internal He–neon laser, and fluorescence emission was observed with a long-pass barrier filter 560DCLP. FITC-ODN and GFP were imaged using the 488-nm excitation line of an argon laser, and fluorescence emission was observed with a filter, HQ515/30.

Association of an FITC-labeled folate-BSA conjugate. Synthesis of an FITC-labeled folate-BSA conjugate (FITC-f-BSA) was carried out.[19] Briefly, folic acid was dissolved in anhydrous dimethylsulfoxide and activated with a five-fold excess of 1-ethyl-3-(3-dimethylaminopropyl)carbodiimide for 1 hour at room temperature. The activated folate was then reacted with FITC-labeled BSA (Sigma Chemical Co.) in phosphate buffer (pH 7.4). Excess folate was removed from conjugated protein using a PD-10 desalting column (Amersham Bioscience Corp., Piscataway, NJ).

PC-3 cells were prepared by plating cells in a 35-mm culture dish 24 hours prior to each experiment. FITC-f-BSA was diluted to 30 μM in 1 ml of folate-deficient RPMI medium containing 10% serum and then incubated with cells in the presence or absence of 1 mM folic acid. After 3 hours incubation, the dishes were washed two times with 1 ml of PBS (pH 7.4) to remove the unbound FITC-f-BSA. FITC-f-BSA was visualized with confocal laser scanning microscopy, as described in the section above.

Immunohistochemistry. Unstained formalin-fixed, paraffin-embedded normal and cancerous prostate tissue slides (Chemicon Select Tissue array: TMA3202, Chemicon International, Temecula, CA) were deparaffinized and rinsed in Tris-buffered saline with 1% Tween 20 (TBST, pH 7.4). Sections were incubated for 1 hour with 1% skim milk in TBST, then rinsed in TBST and again incubated at room temperature with mouse anti-human FR-α monoclonal IgG (Mov18/ZEL, Alexis Biochemicals, San Diego, CA) diluted 1:500 with 1% skim milk in TBST. Next, tissue sections were exposed to FITC-labeled goat anti-mouse IgG Ab (KPL, Guildford, UK) for 1 hour at room temperature. After a wash with TBST, the antigen–antibody complex was visualized with confocal laser scanning microscopy, as described in the section above.

Analysis of GCV metabolites using anion-exchange HPLC. The accumulation of GCV mono-, di- and triphosphate (GCV-MP, GCV-DP and GCV-TP, respectively), in LNCaP and PC-3 cells, was determined using pCMV-tk-transfected cells seeded in a 35-mm culture dish after 24 hours incubation with 100 μg/ml GCV as previously reported.[20] The separation of GCV and its phosphorylated metabolites was performed using a Waters 616 LC HPLC system with UV detection (Milford, MA). The separation of metabolites was accomplished using a Senshu Pak SAX-1253P column (250 × 4.6 mm, Senshu Scientific Co., LTD, Tokyo, Japan).

Sensitivity to the GCV assay. LNCaP and PC-3 cells were seeded at a density of 1×10^4 cells per well in 96-well plates and maintained for 12 hours before transfection in folate-deficient RPMI medium supplemented with 10% serum. The cells were transfected with the NP-F nanoplexes of the 0.2 μg pGL3-enhancer as a control DNA, 0.1 μg pCMV-tk plus 0.1 μg pGL3-enhancer (Promega), 0.1 μg pGL3-enhancer plus 0.1 μg pSV40-Cx43 and 0.1 μg pCMV-tk plus 0.1 μg pSV40-Cx43. After 12 hours incubation, the culture medium was replaced with medium containing various concentrations of GCV ranging from 0.1 to 1000 μg/ml. The number of surviving cells was determined by a WST-8 assay (Dojindo Laboratories, Kumamoto, Japan) after 4 days exposure to GCV.

In vivo *experiments*

Xenograft tumor model. Male BALB/c nu/nu mice (8 weeks of age, CLEA Japan Inc., Tokyo, Japan) were maintained on a folate-deficient rodent diet (Oriental Yeast Co., LTD, Tokyo, Japan) on arrival and for the duration of the study. To generate KB tumor xenografts, 1×10^7 cells suspended in 50 μl of RPMI medium were inoculated subcutaneously in the flank region of the mice. To generate LNCaP tumor xenografts, 1×10^7 LNCaP cells suspended in 50 μl of RPMI medium containing 60% reconstituted basement membrane (Matrigel: Collaborative Research, Bedford, MA) were inoculated subcutaneously into the flank region of the mice. In LNCaP tumor xenografts, to maintain the serum testosterone level, the male mice were i.p. administered 0.5 mg of testosterone propionate (Wako Pure Chemical Industries, Ltd, Osaka, Japan) dissolved in olive oil once every other day. The tumor volume was calculated using the formula tumor volume $= 0.5ab^2$, where a and b are the larger and smaller diameters, respectively.

Luciferase gene transfection. When the volume of the inoculated tumors reached approximately 100 mm^3, 5 μg of pCMV-luc was transfected by direct injection into xenografts with NP-F (24 μl) and Tfx20 (15 μl). After 24 hours, the tumors were excised and immediately homogenized after adding lysis buffer (Promega, Madison, WI) in a volume (μl) equivalent to five times the tissue weight (mg). The tissue homogenate was centrifuged at 20,000 g for 5 minutes after undergoing one round of freeze–thawing. The resulting supernatants were assayed with a luminometer and the luciferase activity was determined in the same manner as *in vitro*.

Assessment of KB or LNCaP tumor growth. When the average volume of KB xenograft tumors reached 150 mm^3 (day 0), these mice were divided into two groups: group I, pGL3-enhancer (10 μg) as a control; group II, pCMV-tk (10 μg). Both experimental groups consisted of six tumors. The NP-F nanoplexes of 10 μg of plasmid per tumor were directly injected into xenografts on days 0, 2, 4 and 6. GCV at a dose of 25 mg/kg was administered i.p. at 24 and 36 hours after the injections of nanoplexes. The tumor volume was measured at days 0, 2, 4, 6, 8, 11 and 13. At day 14, all mice were killed, and the tumor weights and serum concentration of folic acid were measured. The serum concentration of folic acid was determined by a competitive enzyme immunoassay (AIA-Pack folate, Tosoh Co., Tokyo, Japan) on a Tosoh AIA system

analyzer. Tumor volume and weight are shown as the mean±SE and ±SD, respectively.

When the volume of LNCaP xenograft tumors reached 60 mm^3 on average (day 0), these mice were divided into two groups as follows; group I, pGL3-enhancer (10 μg) as a control; and group II, pCMV-tk (5 μg) plus pSV40-Cx43 (5 μg). Each experimental group consisted of six tumors. The NP-F nanoplexes of 10 μg plasmid DNA were transfected by direct injection into xenografts with NP-F (50 μl) on days 0, 3, 5 and 7. GCV at a dose of 25 mg/kg was administered i.p. at 24 and 36 hours after the injection of the nanoplex. The tumor volume was measured on days 0, 3, 5, 7, 9 and 11. The data are shown as the mean±SE. The animal experiments were conducted with ethical approval from our institutional animal care and use committee.

Statistical analysis

The statistical significance of the data was evaluated with Student's *t*-test. A *P*-value of 0.05 or less was considered significant.

Results

Size and ζ-potential of nanoparticles and nanoplexes

We prepared and characterized folate-targeted nanoparticles with four different formulations. All nanoparticle formulations consisted of 1 mg/ml DC-Chol as a cationic lipid, and 5 mol% Tween 80 (NP). In this study, we changed from low-purity to high-purity Tween 80 to improve the transfection efficiency. For FR-targeted vectors, NP-1F, -2F and -3F contained 1, 2 and 3 mol% f-PEG-DSPE, respectively. The average size of each nanoparticle was about 100–200 nm (Table 1). The ζ-potential of NP, NP-1F and -2F was about 53, 44 and 39 mV, respectively, decreasing as the amount of f-PEG-DSPE added increased, except for NP-3F. The physical characteristics of the nanoplex were also investigated at the optimal charge ratio (+/−) of (3/1) of cationic nanoparticle to DNA. When the nanoparticles were mixed with DNA, the size of each nanoplex increased from 200 to 500 nm, and the ζ-potential slightly decreased from +40 to ~ +30 mV. In the presence of 10 and 50% serum, the sizes of the NP, NP-1F and -3F nanoplexes increased up to 500–660 nm, whereas that of NP-2F was 430 nm.

Luciferase expression in cell lines

To optimize the formula of folate-linked nanoparticles, we evaluated the transfection efficiency of NP, NP-1F, NP-2F and NP-3F by measuring luciferase activity in KB, LNCaP and PC-3 cells transfected using pCMV-luc in the presence of 10% serum for 24 hours. Nanoparticles linked to 2 mol% folic acid, NP-2F, showed the highest level of luciferase activity of all the nanoparticles in any cell lines (Fig 1a–c). The optimal folic acid content of nanoparticles was 2 mol%. In subsequent experiments, therefore, we used NP-2F, referred to as NP-F.

To compare the effectiveness of transfection of NP-F with Tfx20, a commercial gene transfection reagent, we measured the luciferase activity in five kinds of cell lines. Compared with Tfx20, NP-F showed five-fold higher transfection efficiency in PC-3 cells, but about 20-fold lower transfection in LNCaP cells (Fig 2a). However, NP-F showed higher transfection efficiencies in LNCaP, PC-3 and HeLa cells than in HepG2 and KB cells.

Expression of FR mRNA in the cell lines

To examine the mechanism of cellular uptake of folate-linked nanoparticles, we investigated the expression of FRs and RFC in the cell lines using the RT-PCR method. There were three FR isoforms, α, β and γ with distinctive patterns of tissue distribution. FR-α mRNA was expressed strongly in KB and HeLa cells, but not expressed in LNCaP, PC-3 or HepG2 cells (Fig 2b). FR-β and -γ mRNAs were not expressed in any of the cell lines (data not shown). RFC, a carrier-mediated folate transporter, was weakly expressed in all cell lines evaluated (Fig 2b). This suggested that the cellular uptake of folate-linked nanoparticles in HeLa and KB cells was mediated via FR-α, following the induction of transfection activity. In HepG2 cells, FR mRNA was not expressed, following the induction of about 100-fold less transfection activity, compared with Tfx20. In LNCaP and PC-3 cells, FR mRNAs were not observed; however, NP-F induced

Table 1 Particle size and ζ-potential of nanoparticles and nanoplexes[a] in the absence and presence of serum

	Nanoparticle			Nanoplex		Nanoplex+10% serum	Nanoplex+50% serum
	Size (nm)		ζ-potential (mV)	Size (nm)	ζ-potential (mV)	Size (nm)	Size (nm)
Formulation	0 days	30 days	0 days	0 days	0 days	0 days	0 days
NP	117.2±2.0	128.8±3.8	53.1±2.5	354.9±8.8	39.0±1.0	510.6±8.4	499.6±38.8
NP-1F	146.1±12.4	142.6±10.3	43.9±1.7	515.2±32.3	34.2±1.6	552.9±49.7	623.2±114.9
NP-2F (NP-F)	165.3±22.1	148.9±7.4	38.6±1.5	233.7±6.5	30.8±1.9	293.3±1.7	431.3±16.0
NP-3F	118.4±4.3	117.4±4.3	54.8±6.3	396.0±7.8	35.1±0.9	482.5±27.7	662.4±7.2

[a]Charge ratio (+/−) of nanoparticle/DNA = 3/1.
NPs consisted of 1 mg/ml DC-Chol and 5 mol% Tween 80 with 0, 1, 2 and 3 mol% f-PEG-DSPE (NP, NP-1F, NP-2F andNP-3F, respectively). Each value represents the mean±SD (n=3).

relatively high levels of transfection, suggesting that the uptake in these cells was mediated by a different mechanism.

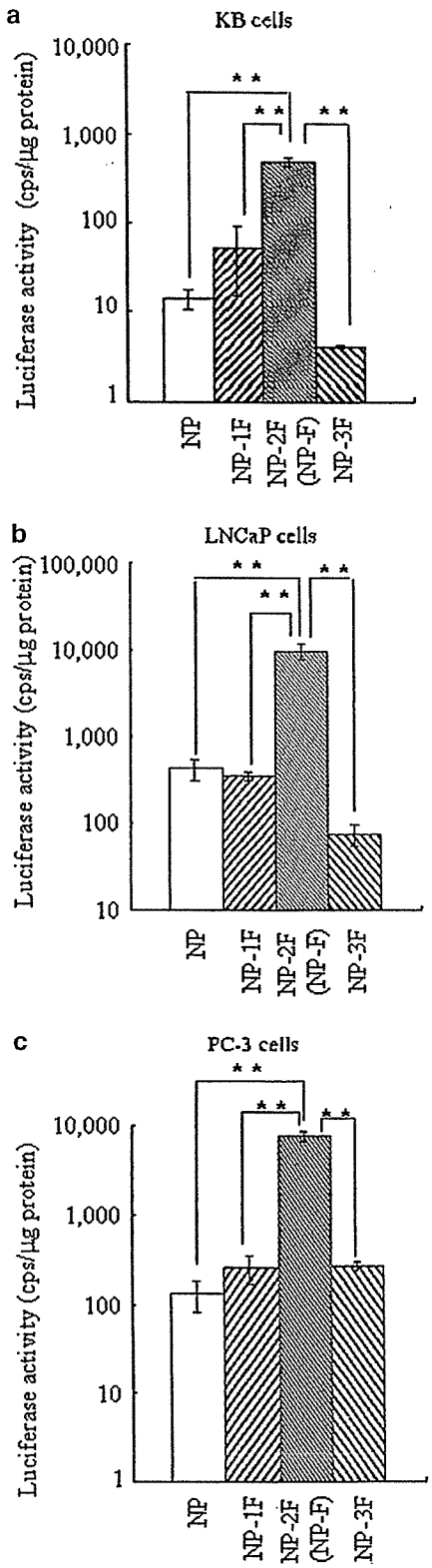

Association of NP-F nanoplex with KB cells

We examined the selectivity of NP-F to carry genes into KB cells using a nonexchangeable fluorescent membrane probe, DiI-labeled NP-F complexed with FITC-ODN, by flow cytometry. As shown in Figure 3a and b, all the cells took up a similar amount of both the fluorescent NP-F and DNA. A comparative experiment in the presence of 1 mM folic acid revealed decreased amount of NP-F and DNA in the cells. These results clearly indicated that the association of NP-F nanoplex with KB cells occurred via FR.

Association of FITC-f-BSA with PC-3 cells and immunohistochemistry

To examine the selectivity of the folate moiety in cellular uptake into PC-3 cells, FITC-f-BSA was visualized by

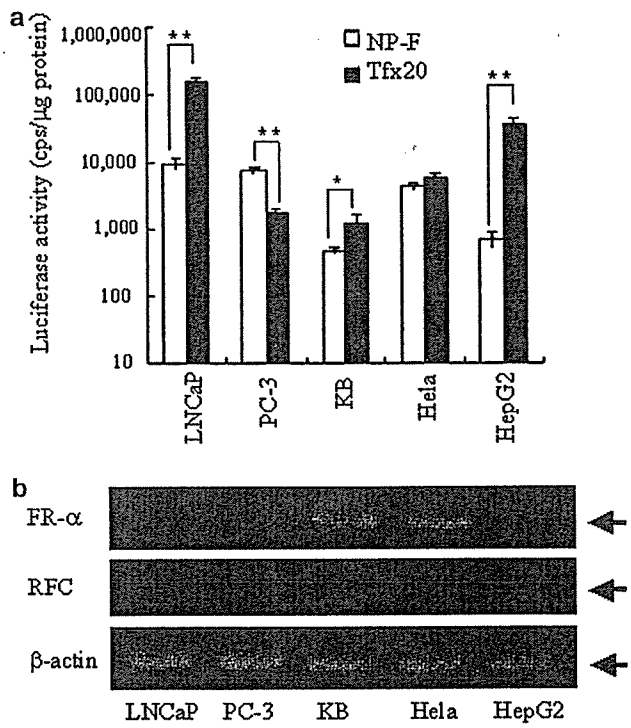

Figure 2 Comparison of transfection efficiencies between NP-F and Tfx20 in the NP-F nanoplexes and Tfx20 lipoplex with pCMV-luc at a charge ratio (+/−) of 3/1 and 2/1, respectively, in various cell lines (**a**). Each column represents the mean±SD ($n=3$). $^{*}P<0.05$, $^{**}P<0.01$. FR-α, RFC and β-actin mRNA expression was detected in various cell lines by RT-PCR (**b**).

Figure 1 Transfection into KB (**a**), LNCaP (**b**) and PC-3 (**c**) cells with various nanoplexes. NP contains no folate-lipid, and nanoparticles containing 1, 2 and 3 mol% f-PEG-DSPE are referred to as NP-1F, NP-2F (NP-F) and NP-3F, respectively. Nanoplexes were prepared by mixing the nanoparticles with pCMV-luc at a charge ratio (+/−) of 3/1. The cells were incubated for 24 hours with nanoplexes of 2 μg DNA/ml in media with 10% serum. The cells were analyzed for luciferase activity. Each column represents the mean±SD ($n=3$). $^{**}P<0.01$, compared with NP-F.

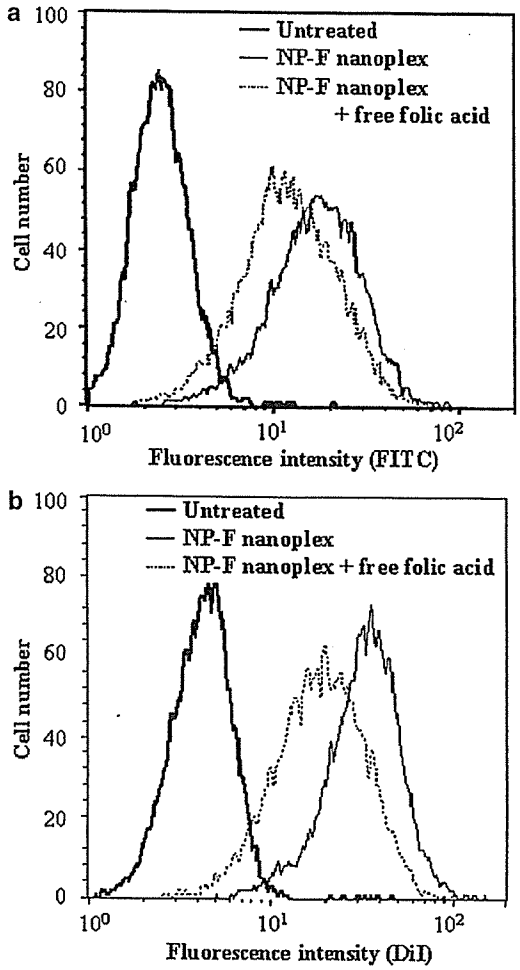

Figure 3 Association of NP-F nanoplex with KB cells. DiI-labeled NP-F was mixed with 2 μg of FITC-ODN at a charge ratio (+/−) of 3/1. The NP-F nanoplex was incubated with cells for 3 hours in the absence or presence of 1 mM free folic acid. The association was determined based on FITC (**a**) and DiI (**b**) fluorescences by flow cytometry, as described in Materials and methods. Flow cytometry of cells exposed to the nanoplex (continuous line) is shown. Dotted line, plus free folic acid; bold line, autofluorescence of the cells.

confocal microscopy. As shown in Figure 4a and b, FICT-f-BSA was associated with the cells. A comparative experiment in the presence of 1 mM folic acid showed a significant decrease in the amount of FICT-f-BSA associated with the cells (Fig 4c and d). These results indicated that the folate moiety accelerated the cellular association of FITC-f-BSA with PC-3 cells.

For an assessment of FR expression in human malignant tumor biopsy specimens, we immunohistochemically stained paraffin-embedded sections for FR-α. In tumor samples, FR-α protein expression was evident in three of four biopsy specimens evaluated (Fig 4e and f). There was positive FR-α staining around the epithelium of the cancerous duct. FR-α mRNA was detected in the RNA from tumor prostate tissue by RT-PCR (data not shown). In contrast, no staining was observed when normal sections were incubated with the FR-α antibody (data not shown).

Transfection efficiency and localization of nanoplexes visualized by confocal microscopy and flow cytometry

To clarify the ability of NP-F to carry genes into LNCaP and PC-3 cells, we examined the efficiency of the transfection of NP-F into LNCaP and PC-3 cells with the pEGFP-C1 plasmid. In both LNCaP (Fig 5a) and PC-3 cells (Fig 5b), strong expression of GFP protein was observed in 2–3% of cells, and weak expression in almost all other cells by confocal microscopy, corresponding to the luciferase expression in both cells (Fig 2a).

Next, we examined the localization of a nonexchangeable fluorescent membrane probe, DiI-labeled NP-F complexed with FITC-ODN, after transfection into LNCaP cells. The distribution pattern of the DiI red signal on NP-F was observed at the cell surface weakly at 3 hours (Fig 5c) and strongly at 24 hours after transfection (Fig 5d). In contrast, the FITC signal was detected throughout the cytoplasm strongly at 3 hours (Fig 5c) and then diffusively at 24 hours after the transfection (Fig 5d). Mostly, the DiI and FITC signals were not colocalized in the cytoplasm. A flow cytometric study also demonstrated that the FITC intensity in LNCaP cells was stronger at 3 hours than at 24 hours after the transfection (Fig 5e), suggesting that the DNA was released from the nanoplex and diffused into the cytoplasm. In PC-3 cells, the signal intensity was also strong at 3 hours after the transfection (data not shown).

In vitro *sensitivity of cells transfected transiently with pCMV-tk and pSV40-Cx43 to GCV*

In order to confirm the transfection of pCMV-tk with NP-F, we analyzed the GCV metabolites in LNCaP and PC-3 cells. GCV-TP, the most abundant triphosphate produced, was clearly detected in the transfected cells, while there was no detectable phosphorylation of GCV in nontransfected cells (data not shown).

Next, LNCaP and PC-3 cells were transiently transfected with the NP-F nanoplex using various plasmids: pCMV-tk, pSV40-Cx43 and combinations thereof (Fig 6). The degree of sensitivity to GCV was compared as the IC_{50}. In LNCaP cells, the pCMV-tk-transfected cells showed significantly higher sensitivity to GCV than the control (85.6-fold increase), or pSV40-Cx43-transfected cells (6.6-fold increase) (Fig 6a). The cells cotransfected with pCMV-tk and pSV40-Cx43 exhibited increased sensitivity to GCV (101.8-fold increase compared with the control). This result suggests that pCMV-tk and pSV40-Cx43 induced a cytotoxic effect by GCV in the transfected cells, and that the combination of pCMV-tk and pSV40-Cx43 may display a bystander effect.

In PC-3 cells, the pCMV-tk-transfected cells showed significant sensitivity to GCV compared with the control (Fig 6b), but the pSV40-Cx43-transfected cells did not. The sensitivity to GCV was not enhanced in the cells transfected with pCMV-tk plus pSV40-Cx43. This result

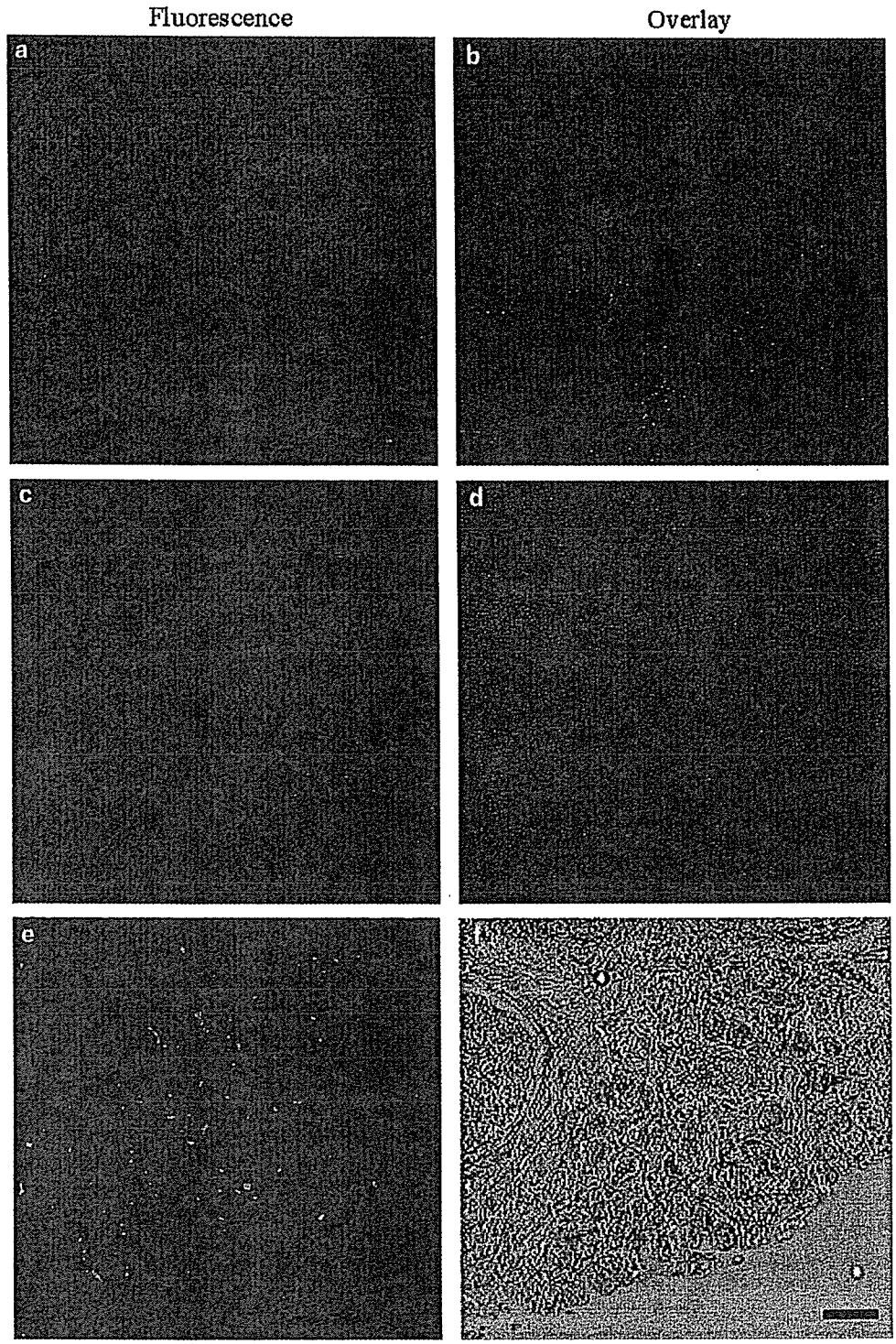

Figure 4 Association of FITC-f-BSA with PC-3 cells. FITC-f-BSA was incubated with cells for 3 hours in the absence (**a, b**) or presence (**c, d**) of free folic acid. The FITC-f-BSA was visualized by confocal microscopy (magnification $\times 600$). Immunohistochemical staining of FR-α in a malignant prostate tumor (**e, f**). The FITC-labeled antibody was visualized by confocal microscopy (magnification $\times 300$). The picture in the left panel corresponds to the fluorescence image. The corresponding transmission image overlaid with the fluorescence image is presented in the right panel. Scale bar = 50 μm.

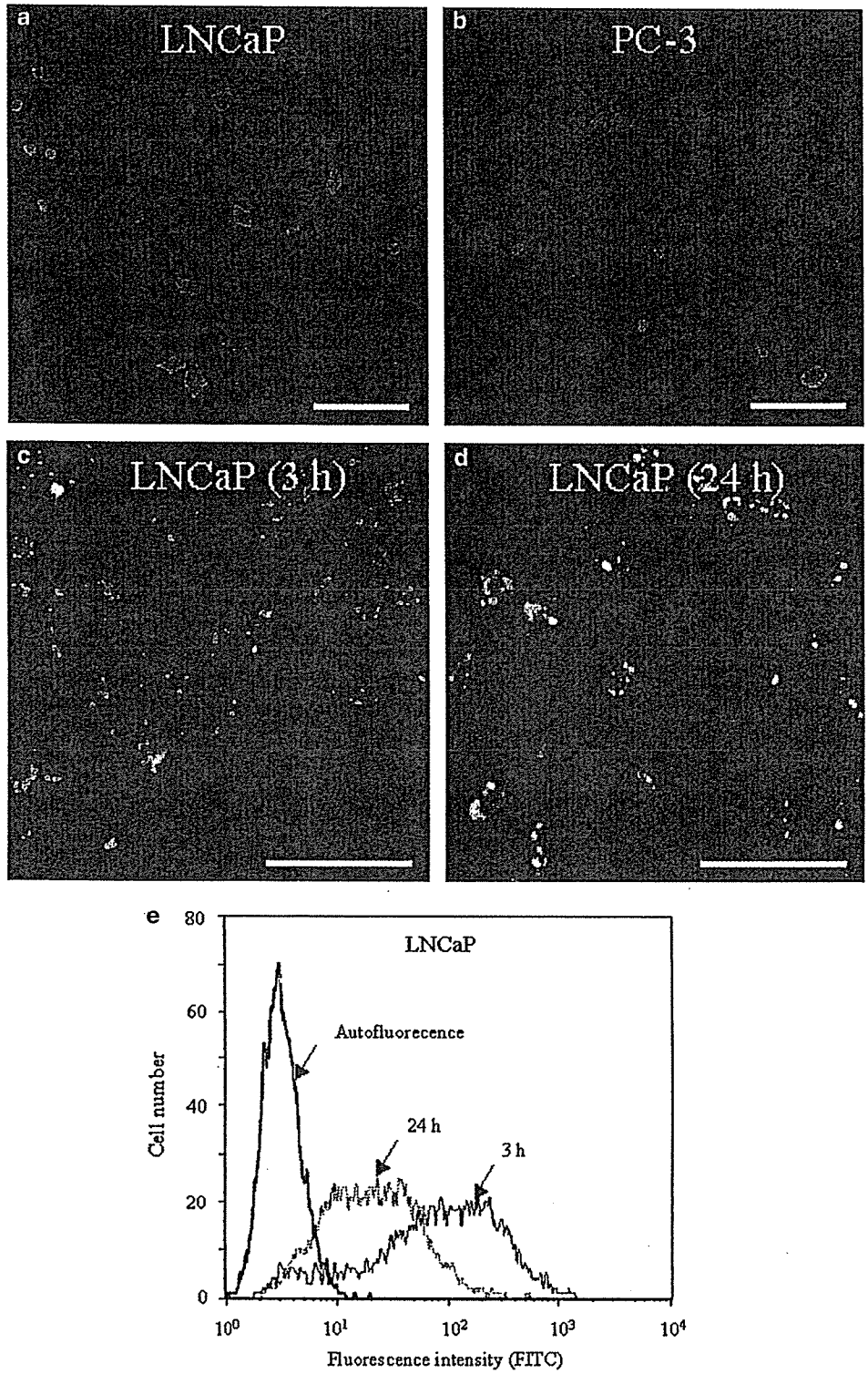

Figure 5 Uptake and expression of DNA with NP-F nanoplex in LNCaP and PC-3 cells. In panels **a** and **b**, NP-F mixed with the pEGFP-C1 plasmid was incubated with LNCaP (a) and PC-3 (b) cells for 24 hours. Expression of GFP protein was visualized by confocal microscopy (magnification × 600). In panels **c** and **d**, DiI-labeled NP-F mixed with FITC-ODN was incubated with LNCaP cells for 3 hours (**c**) or 24 hours (**d**). DiI-labeled NP-F and FITC-ODN were visualized by confocal microscopy (magnification × 1000). The red signals show the localization of DiI-labeled NP-F, and the green signals show that of FITC-ODN. Scale bar = 50 μm. In panel **e**, the association of DNA with NP-F was determined based on FITC-ODN by flow cytometry. Flow cytometry of autofluorescence of the cells (bold line), and the cells exposed to the nanoplex for 3 hours (continuous line) and for 24 hours (dotted line).

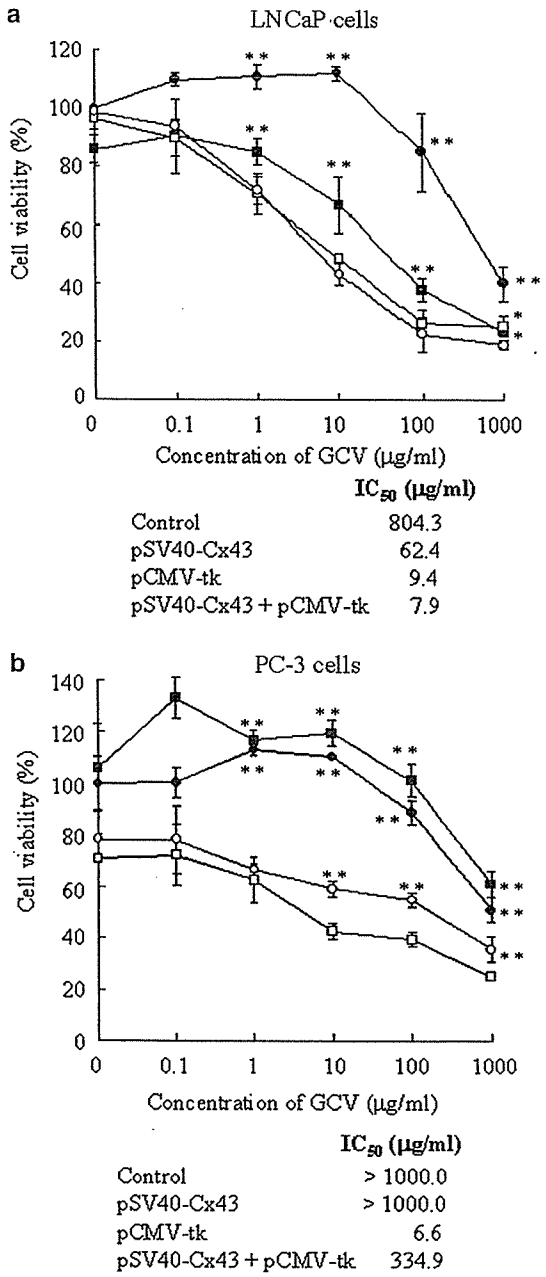

Figure 6 Sensitivity of LNCaP (**a**) and PC-3 (**b**) cells to GCV. The cells were transfected with various plasmids using NP-F. After 12 hours incubation, the medium was changed to one containing GCV. The plasmids used were pGL3-enhancer as a control plasmid (●), pCMV-tk (○), pSV40-Cx43 (■) and pCMV-tk plus pSV40-Cx43 (□). Data points indicate the mean±SD ($n=3$). *$P<0.05$ and **$P<0.01$, compared with pCMV-tk and pSV40-Cx43 in (**a**). *$P<0.05$ and **$P<0.01$, compared with pCMV-tk in (**b**).

suggests that pSV40-Cx43 did not display a bystander effect in PC-3 cells.

Luciferase expression in the xenografts

To evaluate the transfection efficiency of NP-F in KB tumor xenografts, we measured luciferase activity after direct injection of NP-F nanoplex into xenografts compared with Tfx20. NP-F showed about 100 times higher transfection than Tfx20 *in vivo* (data not shown).

In vivo *suicide gene therapy in KB or LNCaP tumor xenografts*

We evaluated the antitumor effect by direct injection into KB tumor xenografts with the NP-F nanoplex of pCMV-tk. When KB cells were transiently transfected with the NP-F nanoplex using various plasmids, pCMV-tk, pSV40-Cx43 and combinations thereof, the pCMV-tk-transfected cells showed significant sensitivity to GCV compared with the control, but did not with the cells cotransfected with pCMV-tk and pSV40-Cx43 (data not shown). Therefore, NP-F nanoplex of pCMV-tk was used in KB tumor xenografts. The growth of KB tumors was significantly inhibited in the mice treated with the NP-F nanoplex (Fig 7a) on day 13. A comparison of tumor weight and appearance after excision also demonstrated that the tumor growth was attenuated in the mice treated with the nanoplex of pCMV-tk (Fig 7b and c). In the mice fed a folate-deficient diet, the serum concentrations of folic acid were approximately 50 nM, which was significantly lower than the concentration in the mice fed a normal diet (200 nM) (data not shown).

Next, we evaluated the antitumor effect by direct injection into LNCaP tumor xenografts with the NP-F nanoplex of pCMV-tk plus pSV40-Cx43 (Fig 8), because this nanoplex was the most effective in the *in vitro* experiments with LNCaP cells (Fig 6a). Tumor growth was suppressed in the mice treated with the NP-F nanoplex of pCMV-tk plus pSV40-Cx43, but not in the control mice. The mean survival times of the control mice and the mice treated with the nanoplex of pCMV-tk plus pSV40-Cx43 were 21.5 and 33 days, respectively (data not shown).

Discussion

One major problem in gene therapy is how to transfect target cells efficiently and specifically. Previously, we reported that the NP-1F vector, composed of 94 mol% DC-Chol, 5 mol% conventional Tween 80 (about 50% pure; Tokyo Kasei Kogyo Ltd, Tokyo, Japan) and 1 mol% f-PEG-DSPE, exhibited selective uptake in KB cells *in vitro*, but had less transfection efficiency than Tfx20.[17] In the present study, we changed from low-purity to high-purity Tween 80 (99% pure). NP-2F (NP-F), composed of 93 mol% DC-Chol, 5 mol% high-purity Tween 80 and 2 mol% f-PEG-DSPE, exhibited five times higher transfection efficiency than the NP-1F prepared in the previous study (0.2×10^3 cps/μg protein).[17] Furthermore, NP-F formed an injectable nanoplex of about 200 nm (Table 1), even in the presence of serum, did not aggregate and maintained its size (about 400 nm). This suggests the usefulness of NP-F as a selective and high-transfection vector *in vivo* for cancer cells overexpressing FR. High-purity Tween 80 may provide greater steric

stabilization and stronger fusogenic activity in the particles.[21] This could be one of the reasons why high levels of transfection activity were observed in the formula difference between the previous[17] and present study.

A reduction in the ζ-potential with the addition of f-PEG-DSPE was not observed in NP-3F (about 55 mV). f-PEG-DSPE might not be incorporated into NP-3F particles. The concentration of folate-PEG_{2000}-DSPE in NP-2F and 3F was about 40 and 60 μM, respectively. f-PEG-DSPE below the critical micelle concentration (CMC) might lead to an efficient incorporation into the particles. However, f-PEG-DSPE above the CMC may help to stabilize micellized f-PEG-DSPE and to inefficient insertion into the particle. The CMC of f-PEG-DSPE may be between 40 and 60 μM and might affect the incorporation of f-PEG-DSPE in NP-3F.

We optimized the nanoparticle formula, 2 mol%–folate-linked, NP-F, by evaluating the transfection efficiency of 1–3 mol% folate-linked nanoparticles since NP-F showed significantly high DNA transfection in KB, LNCaP and PC-3 cells (Fig 1a–c). In prostate cancer, there have been no reports of the expression of FR in either cultured human prostate cell lines or tissue specimens, and an evaluation of the expression of FR mRNAs by RT-PCR indicated an absence of FR mRNAs in LNCaP and PC-3 cells (Fig 2b). However, NP-F showed relatively high transfection activity in prostate cancer cells

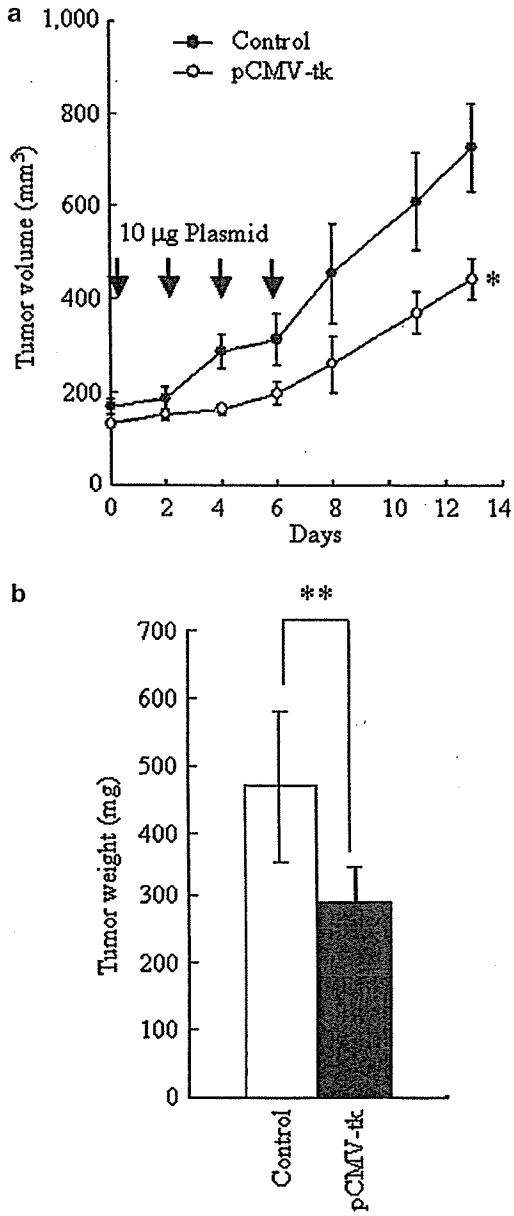

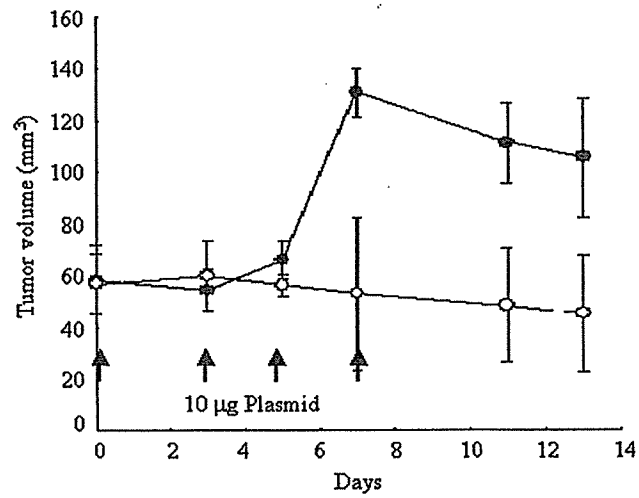

Figure 8 Suicide gene therapy of LNCaP tumor xenografts with GCV in mice. Mice were divided into two groups: group I, pGL3-enhancer (●) as a control; group II, pCMV-tk plus pSV40-Cx43 (○). The NP-F nanoplexes of the plasmids indicated were injected directly into the tumor four times (day 0, 3, 5 and 7). GCV (25 mg/kg) was administered i.p. at 24 and 36 hours after the injections of nanoplexes. The results indicate the mean volume ± SE ($n=6$).

Figure 7 *In vivo* suicide gene therapy of KB tumor xenografts with GCV in mice. Mice were divided into two groups: group I, pGL3-enhancer (10 μg) as a control; group II, pCMV-tk (10 μg). The NP-F nanoplexes of the plasmids were injected directly into the tumor four times (day 0, 2, 4 and 6). GCV (25 mg/kg) was administered i.p. at 24 and 36 hours after the injections of nanoplexes. Tumor volume (**a**), excised tumor weight (**b**) and macroscopic tumor appearance (**c**) when all mice in (**a**) were killed at day 14. The results indicate the mean volume and weight ± SE or ± SD, respectively ($n=5$). $^{*}P<0.05$ and $^{**}P<0.01$, compared with control.

compared to KB and HeLa cell lines, which strongly expressed FR-α mRNA (Fig 2a). This suggests the usefulness of NP-F as an effective DNA transfection reagent for the prostate androgen-dependent and -independent cancer cells.

The FR-specific delivery with the NP-F nanoplex in KB cells was compared in the absence or presence of 1 mM folic acid in the medium. The association of the nanoplex with the cells was reduced in the presence of free folic acid (Fig 3a and b). This suggests that an association via interaction between the folate moiety of NP-F and FR of KB cells is a major route of NP-F nanoplex transfection, corresponding with a previous study.[22] In the human prostate, high-affinity folate binding protein was characterized,[16] and folic acid binds to the membrane fraction that crossreacts with the anti-prostate-specific membrane antigen (PSMA) antibody.[23] PSMA is a transmembrane protein with an overexpressed pattern restricted to malignant human prostate tissue and LNCaP cells.[24] The physiological role of PSMA in prostate cancer remains unknown, but PSMA shows hydrolase enzymatic activity with a folate substrate[23] and is internalized via an endocytic mechanism.[25] If PSMA functions as a receptor mediating the internalization of a putative ligand similar to folic acid, this suggests that the folate-linked nanoparticle binds to PMSA and is then taken up via an endocytic mechanism by LNCaP cells as we reported.[17] In PC-3 cells, our study using RT-PCR confirmed the presence of RFC mRNA, but found no FR or PSMA mRNAs (data not shown). However, FITC-f-BSA was taken up by PC-3 cells and the cellular association was significantly decreased in the presence of 1 mM folic acid (Fig 4a–d). We cannot exclude the possibility that the uptake of NP-F in PC-3 cells was mediated by RFC; however, it is not clear what kind of receptor enhances the uptake of folate-linked nanoparticles.

In prostate cancer, we observed potential discrepancies between cultured cells and tissue specimens in the expression of FR. We found that FR-α protein was expressed in cancerous tissue (Fig 4e and f), but not in LNCaP or PC-3 cells (Fig 2b). Immunohistochemistry indicated the expression of FR-α around the epithelium of the cancerous duct, but not in the normal prostate tissues evaluated in the present study. Therefore, NP-F will be potentially useful as a prostate tumor-specific vector via FR for *in vivo* gene therapy. Further studies will be required to determine the relationship between normal and malignant prostate tissue specimens in the expression of FR.

The HSV-tk/GCV therapy system relies on the expression of the exogenous HSV-tk gene in the cancer cells. HSV-tk gene expression was confirmed by the production of GCV metabolites (data not shown) and cell growth inhibition in the presence of GCV (Fig 6). HSV-tk-expressing cells can induce the death of nonexpressing neighbors via gap junctions (bystander effect).[7,26] In the normal human prostate, the cells communicate via gap junctions, whereas, in poorly differentiated prostate cancer, the expression of Cx43 decreased and gap junctional intracellular communication failed.[8,9] Transfection of the Cx43 gene into Cx43-deficient LNCaP cells may enhance the bystander effect, and was reported to inhibit cell growth, retard tumorigenicity and induce differentiation.[27]

In LNCaP cells, the pCMV-tk-transfected cells showed significant sensitivity to GCV compared with the control (Fig 6a). Although the pSV40-Cx43-transfected cells did not show growth inhibition without GCV, they showed significant sensitivity similar to the pCMV-tk-transfected cells at high concentrations of GCV. Connexins assembled into hexamers insert into the plasma membrane, and dock in an opposed membrane to form gap junction channels.[28] It is generally assumed that the surface expression of an unjunctional channel, a hemichannel, is closed to prevent metabolic stress and death caused by the collapse of the ionic gradient and influx of Ca^{2+}, but it can be opened under physiological and pathological conditions.[29] In the pSV40-Cx43-transfected cells, the hemichannel might be opened by unknown factors, and induce intracellular influx of a large amount of GCV. Since with a high concentration of GCV, nonphosphated GCV showed cytotoxicity in the control cells, the cytotoxicity in pSV40-Cx43-transfected cells might be caused by the intracellular influx of GCV, even at low concentrations of GCV. The cells transfected with pCMV-tk plus pSV40-Cx43 had increased sensitivity to GCV, compared with those transfected with only pSV40-Cx43 or pCMV-tk. This may be due to an enhanced cytotoxic effect by GCV metabolites and a bystander effect on transfection.

In PC-3 cells, the pCMV-tk-transfected cells showed significant sensitivity to GCV compared with the control (Fig 6b). In contrast, the cells transfected with pCMV-tk plus pSV40-Cx43 did not exhibit an increase in sensitivity to GCV compared with pCMV-tk-transfected cells. The expression of Cx43 in LNCaP cells may induce the formation of gap junctions, but that in PC-3 cells may not,[30] suggesting the absence of a bystander effect.

The major limitation of *in vivo* gene therapy using liposomes is the low transfection efficiency. Comparing transfection efficiency in KB xenograft tumors in mice between NP-F and Tfx20, the luciferase activity by NP-F was about 100-fold higher than that by Tfx20 (data not shown), suggesting that the NP-F nanoplex remained small enough to migrate into the tumorous tissue. Plasma folic acid may interfere with the binding of FR. The human serum folic acid concentration, following the recent FDA-mandated dietary supplementation, is ~42 nM.[31] Earlier reports indicated that serum folic acid at this concentration should not significantly inhibit the binding of FR mediated by liposomes.[22] Results of the present study showed that the mice were actually able to maintain a plasma folate level within the physiologic range of humans on a folate-deficient diet. In contrast, the mice on a normal diet maintained a much higher serum concentration of folic acid. The results of this study, therefore, should be considered relevant to humans with respect to serum folate levels.

In gene therapy *in vivo*, we demonstrated that the NP-F nanoplex of pCMV-tk followed by GCV treatment could

significantly suppress the growth of KB tumor xenografts (Fig 7a–c). The combination of pCMV-tk and pSV40-Cx43 suppressed LNCaP tumor growth *in vivo* compared with the control (Fig 8). The observed reduction in tumor size may not be wholly due to the direct effect of the phosphorylated GCV on the transduced tumor cells. An indirect mechanism (the bystander effect) might be contributing to the antitumor activity. It is reported that a 1–5% *in vivo* transfection efficiency could generate a significant antitumor effect in suicide gene therapy.[32] In our study, we observed the strong expression of GFP by NP-F in 2–3% of prostate cancer cells, and a weak expression in almost all other cells (Fig 5a). Moreover, we demonstrated that the NP-F nanoplex showed strong luciferase activity in KB tumor xenografts (data not shown). Therefore, we believe that the transfection efficiency of NP-F is sufficient to inhibit cell growth *in vivo*.

In this study, we showed that folate-linked nanoparticles could effectively deliver genes in human prostate cancer and nasopharyngeal cancer cells, resulting in an increase in sensitivity of both cells to GCV. In suicide gene therapy, transfection of pCMV-tk by NP-F and GCV treatment could suppress the growth of LNCaP and KB tumor xenografts. Furthermore, we detected the expression of FR protein immunohistochemically in human prostate cancer biopsy specimens. These findings indicate that folate-linked nanoparticles have potential as a clinically effective vector in prostate and nasopharyngeal cancer suicide gene therapy.

Acknowledgments

We thank Dr Kazuhiro Kubo (NOF Corporation, Tokyo, Japan) for supplying amino-PEG-DSPE. This project was supported in part by a grant from the Promotion and Mutual Aid Corporation for Private Schools of Japan, and by a Grant-in-Aid for Scientific Research from the Ministry of Education, Culture, Sports, Science, and Technology of Japan.

References

1. Gao X, Porter AT, Grignon DJ, et al. Diagnostic and prognostic markers for human prostate cancer. *Prostate.* 1997;31:264–281.
2. Ellis WJ, Vessella RL, Buhler KR, et al. Characterization of a novel androgen-sensitive, prostate-specific antigen-producing prostatic carcinoma xenograft: LuCaP 23. *Clin Cancer Res.* 1996;2:1039–1048.
3. Mabjeesh NJ, Zhong H, Simons JW. Gene therapy of prostate cancer: current and future directions. *Endocr Relat Cancer.* 2002;9:115–139.
4. Yoshimura I, Suzuki S, Tadakuma T, Hayakawa M. Suicide gene therapy on LNCaP human prostate cancer cells. *Int J Urol.* 2001;8:S5–S8.
5. Hall SJ, Mutchnik SE, Yang G, et al. Cooperative therapeutic effects of androgen ablation and adenovirus-mediated herpes simplex virus thymidine kinase gene and ganciclovir therapy in experimental prostate cancer. *Cancer Gene Ther.* 1999;6:54–63.
6. Fillat C, Carrio M, Cascante A, Sangro B. Suicide gene therapy mediated by the Herpes Simplex virus thymidine kinase gene/Ganciclovir system: fifteen years of application. *Curr Gene Ther.* 2003;3:13–26.
7. Mesnil M, Piccoli C, Tiraby G, et al. Bystander killing of cancer cells by herpes simplex virus thymidine kinase gene is mediated by connexins. *Proc Natl Acad Sci USA.* 1996; 93:1831–1835.
8. Tsai H, Werber J, Davia MO, et al. Reduced connexin 43 expression in high grade, human prostatic adenocarcinoma cells. *Biochem Biophys Res Commun.* 1996;227:64–69.
9. Habermann H, Ray V, Habermann W, Prins GS. Alterations in gap junction protein expression in human benign prostatic hyperplasia and prostate cancer. *J Urol.* 2002;167: 655–660.
10. Campbell IG, Jones TA, Foulkes WD, Trowsdale J. Folate-binding protein is a marker for ovarian cancer. *Cancer Res.* 1991;51:5329–5338.
11. Wu M, Gunning W, Ratnam M. Expression of folate receptor type alpha in relation to cell type, malignancy, and differentiation in ovary, uterus, and cervix. *Cancer Epidemiol Biomarkers Prev.* 1999;8:775–782.
12. Ni S, Stephenson SM, Lee RJ. Folate receptor targeted delivery of liposomal daunorubicin into tumor cells. *Anticancer Res.* 2002;22:2131–2135.
13. Reddy JA, Abburi C, Hofland H, et al. Folate-targeted, cationic liposome-mediated gene transfer into disseminated peritoneal tumors. *Gene Therapy.* 2002;9:1542–1550.
14. Hofland HE, Masson C, Iginla S, et al. Folate-targeted gene transfer *in vivo*. *Mol Ther.* 2002;5:739–744.
15. Ward CM. Folate-targeted non-viral DNA vectors for cancer gene therapy. *Curr Opin Mol Ther.* 2000;2:182–187.
16. Holm J, Hansen SI, Hoier-Madsen M. High-affinity folate binding in human prostate. *Biosci Rep.* 1993;13:99–105.
17. Hattori Y, Maitani Y. Enhanced *in vitro* DNA transfection efficiency by novel folate-linked nanoparticles in human prostate cancer and oral cancer. *J Control Rel.* 2004;97:173–183.
18. Miyauchi M, Yoshida Y, Tada Y, et al. Expression of herpes simplex virus-thymidine kinase gene controlled by a promoter region of the midkine gene confers selective cytotoxicity to ganciclovir in human carcinoma cells. *Int J Cancer.* 2001;91:723–727.
19. Turek JJ, Leamon CP, Low PS. Endocytosis of folate–protein conjugates: ultrastructural localization in KB cells. *J Cell Sci.* 1993;106:423–430.
20. Agbaria R, Candotti F, Kelley JA, et al. Biosynthetic ganciclovir triphosphate: its isolation and characterization from ganciclovir-treated herpes simplex thymidine kinase-transduced murine cells. *Biochem Biophys Res Commun.* 2001;289:525–530.
21. Kim TW, Chung H, Kwon IC, et al. Optimization of lipid composition in cationic emulsion as *in vitro* and *in vivo* transfection agents. *Pharm Res.* 2001;18:54–60.
22. Lee RJ, Low PS. Delivery of liposomes into cultured KB cells via folate receptor-mediated endocytosis. *J Biol Chem.* 1994;269:3198–3204.
23. Pinto JT, Suffoletto BP, Berzin TM, et al. Prostate-specific membrane antigen: a novel folate hydrolase in human prostatic carcinoma cells. *Clin Cancer Res.* 1996;2: 1445–1451.
24. Silver DA, Pellicer I, Fair WR, et al. Prostate-specific membrane antigen expression in normal and malignant human tissues. *Clin Cancer Res.* 1997;3:81–85.

25. Rajasekaran SA, Anilkumar G, Oshima E, et al. A novel cytoplasmic tail MXXXL motif mediates the internalization of prostate-specific membrane antigen. *Mol Biol Cell.* 2003;14:4835–4845.
26. Hamel W, Magnelli L, Chiarugi VP, Israel MA. Herpes simplex virus thymidine kinase/ganciclovir-mediated apoptotic death of bystander cells. *Cancer Res.* 1996;56:2697–2702.
27. Mehta PP, Perez-Stable C, Nadji M, et al. Suppression of human prostate cancer cell growth by forced expression of connexin genes. *Dev Genet.* 1999;24:91–110.
28. Contreras JE, Saez JC, Bukauskas FF, Bennett MV. Gating and regulation of connexin 43 (Cx43) hemichannels. *Proc Natl Acad Sci USA.* 2003;100:11388–11393.
29. Musil LS, Goodenough DA. Biochemical analysis of connexin43 intracellular transport, phosphorylation, and assembly into gap junctional plaques. *J Cell Biol.* 1991;115:1357–1374.
30. Govindarajan R, Zhao S, Song XH, et al. Impaired trafficking of connexins in androgen-independent human prostate cancer cell lines and its mitigation by alpha-catenin. *J Biol Chem.* 2002;277:50087–50097.
31. Lawrence JM, Petitti DB, Watkins M, et al. Trends in serum folate after food fortification. *Lancet.* 1999;354:915–916.
32. Huber BE, Austin EA, Richards CA, et al. Metabolism of 5-fluorocytosine to 5-fluorouracil in human colorectal tumor cells transduced with the cytosine deaminase gene: significant antitumor effects when only a small percentage of tumor cells express cytosine deaminase. *Proc Natl Acad Sci USA.* 1994;91:8302–8306.

Folate-Linked Lipid-Based Nanoparticle for Targeted Gene Delivery

Yoshiyuki Hattori and Yoshie Maitani*

Institute of Medicinal Chemistry, Hoshi University, Ebara 2-4-41, Shinagawa-ku, Tokyo 142-8501, Japan

Abstract: Cancer gene therapy has been intensively developed using non-viral vectors, among which cationic liposomes and nanoparticles are the most thoroughly investigated. For targeted delivery to tumors, vitamin folic acid has been utilized for folate receptor (FR)-mediated drug delivery, since FR is frequently overexpressed on many types of human tumors. Liposomes conjugated to folate ligand have been used as carriers of chemotherapeutic agents and DNA to receptor-bearing tumor cells *in vitro*. As an alternative treatment for prostate cancer, suicide gene therapy by local injection using an adenoviral vector has been reported, but not that using non-viral vectors. The folate-linked, lipid-based nanoparticles which we developed could deliver genes extensively to FR-negative LNCaP and PC-3 cells, as well as FR-positive KB and Hela cells. In this review, we outline folate-linked liposomes and nanoparticles, and show the effectiveness of folate-linked, lipid-based nanoparticles as a vector for DNA transfection and for suicide gene therapy, to treat human nasopharyngeal and prostate tumors.

Keywords: Cationic nanoparticles, folic acid, gene therapy, thymidine kinase, ganciclovir, prostate cancer, cancer therapy.

INTRODUCTION

Cancer gene therapy has been intensively developed using non-viral vector [1]. Viral vectors such as retroviruses [2], adenoviruses [3], adeno-associated viruses [4] and several other viral types [5], are efficient in transfection, but pose risks to the host from the immunogenicity of viral proteins, a lack of desired tissue selectivity, the potential for oncogenesis due to chromosomal integration, and the generation of infectious viruses due to recombination, making non-viral vectors an attractive alternative. Synthetic vectors such as cationic polymers, liposomes and nanoparticles, have been widely studied for DNA delivery due to their potential for tissue-specific targeting, their lack of immunogenicity, the relative safety, and relative ease of large-scale production. For targeted delivery to tumors, vitamin folic acid has been utilized for folate receptor (FR)-mediated drug delivery, since the FR is frequently overexpressed in human tumors [6,7]. Liposomes conjugated to folate ligand have been reported as carriers of chemotherapeutic agents to FR-bearing tumor cells *in vivo* [8-14]. While much has been published on folate-drug conjugates and folate-linked carriers, relatively little is known about the targeting of gene delivery. The use of a folate ligand as a targeting ligand to deliver DNA has also been reported *in vitro* [15-19], but not been successful in *in vivo* gene therapy [20,21]. Therefore, in this review, we describe the current understanding of folate-linked lipid-based vectors, liposomes and nanoparticles. Information pertaining to the transfection activity by folate-linked lipid-based nanoparticles from suicide gene therapy to treat prostate and nasopharyngeal tumors *in vivo* is also included.

*Address correspondence to this author at the Institute of Medicinal Chemistry, Hoshi University, Ebara 2-4-41, Shinagawa-ku, Tokyo 142-8501, Japan; Tel:/Fax: +81-3-5498-5048; E-mail: yoshie@hoshi.ac.jp

FOLATE RECEPTORS

Folate, as a low molecular weight agent possessing high affinity for FR, has several advantages as a targeting ligand. Folate is stable and lacks immunogenicity. FR-targeting materials can continuously accumulate into cells due to receptor recycling. FR-targeting imaging agents arrived in the market in 2004. FR has been found to be overexpressed in a wide range of tumors [6,7], and is known as a high-affinity membrane, folate-binding protein, which mediates uptake of the vitamin by receptor-mediated endocytosis [22]. Therefore, it presents an attractive target for tumor-selective delivery. Three isoforms of FR have been identified and two, FR-α and -β, are attached to the cell by a glycosylphosphatidylinositol (GPI)-anchor, while FR-γ is secreted due to the lack of an efficient signal for GPI modification [7]. The role of FRs in the cellular transport of folate is not well-understood, although a potocytosis (caveolin-coated endocytosis) model has been proposed [22]. FR-α was found to be clustered in membrane region called caveolae [22]. While an elevated expression of FR has frequently been observed in various types of human tumors, the receptor is generally absent in normal tissues with the exception of the choroid plexus and placenta, with low levels in the lung, thyroid and kidney [23]. FR-α is frequently overexpressed in tumors, including ovarian, endometrial, colorectal, breast, lung, renal cell carcinomas and brain metastases derived from epithelial cancers [6,7]. FR-β is frequently overexpressed in tumors of non-epithelial cell lineages such as sarcomas and acute myeloid leukemia [24], and FR-γ is overexpressed in malignant hematopoietic cells [25]. The causes of FR overexpression in tumors are unclear, but high levels of FR may be associated with increased biological aggressiveness of carcinomas.

FOLATE RECEPTOR TARGETING VECTORS

A major focus in the search for vectors for gene therapy has been tissue-specific targeting for safety. The performance

1567-2018/05 $50.00+.00